Mismatch in nematic interactions leads to composition-dependent crystal nucleation in polymer blends

Wenlin Zhang* and Lingyi Zou

Department of Chemistry, Dartmouth College, Hanover, New Hampshire 03755, United States

E-mail: wenlin.zhang@dartmouth.edu

Abstract

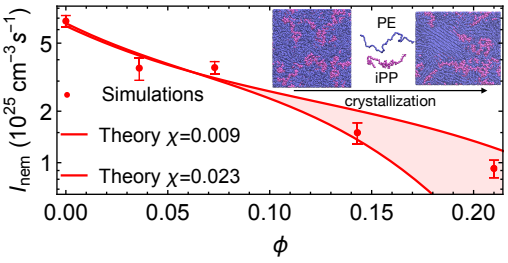

For Table of Contents use only

We employ molecular dynamics (MD) simulations to study the crystal nucleation in polymer blends consisting of high-density polyethylene (PE) and small amounts of impurity polymers. In strongly phase-separated blends, we show crystal nucleation occurs in the PE domain with a rate identical to that in pure samples. Crystal nucleation from well-mixed melts, however, is composition-dependent. Combining simulation results with a mean-field theory, we demonstrate that the composition dependence of crystal nucleation rate arises from the mismatch in nematic interactions of PE and the

impurities. Impurities with weaker nematic interactions, such as isotactic polypropylene, can enhance the free energy barrier of nematic precursor formation, a prerequisite for PE to nucleate crystalline order under strong supercooling conditions. The slower formation of nematic precursors leads to reduced crystal nucleation rates as the impurity volume fraction increases. Polymers with sufficiently strong nematic interactions, such as trans-1,4-polybutadiene, however, impose negligible effects on PE crystal nucleation. We expect our findings to inspire the development of quantitative theories for predicting crystallization in the bulk and interfacial regions of polymer blends, such as mechanically recycled plastics.

Introduction

Crystallization is critical to the performance of semicrystalline polymers, ranging from advanced functional polymers to recycled commodity plastics. Different processing histories can lead to various degrees of crystallinity, and sizes and distributions of crystalline domains inter-connected by amorphous tie-chains. The detailed semicrystalline structures govern the mechanical, optical, and electronic properties of polymeric materials.[1–3] A fundamental understanding of the crystallization mechanisms is necessary for quantitatively controlling crystallization behaviors and the resulting material properties.

Indeed, the mechanisms for a single polymer species to crystallize from melts or solutions have been studied intensively. Previous authors have proposed various theories to qualitatively describe the crystallization process based on experimental observations.[4–7] To develop more quantitative models and reveal nucleation and crystallization behaviors at the microscopic level, molecular dynamics (MD) simulations are also employed to investigate quiescent and flow-induced polymer crystallization. For example, previous work demonstrated the important roles of precursors, nematic ordering, and molecular entanglement in polymer crystal nucleation.[8–14]

Crystallization in polymer blends and block copolymers, however, is still not well understood. In these materials, crystallization and liquid-liquid phase separation can cooperatively affect morphology evolution. Using polarized optical microscopy (POM) and differential scanning calorimetry (DSC), previous work demonstrated that spinodal decomposition could promote crystallization in some incompatible polyolefin copolymer blends under shallow supercooling conditions.[15–21] In this case, crystallization from a phase-separating blend is faster than that in a pure sample and the crystalline spherulites prefer to form near the interfaces between different polymer domains. To rationalize the experimental observations, Mitra and Muthukumar proposed a heterogeneous nucleation model, in which the interfaces between two polymers act as nucleation agents.[22] However, in some other polymer blends, interfaces between different polymer domains may hinder crystal nucleation at low crystal-

lization temperatures so that the crystalline order prefers to grow in the center of phase-separated domains.[23] Quantitative studies of the composition-dependent crystallization in polymer blends and block copolymers, especially for well-mixed or weakly phase-separated systems, are still mostly lacking.

In this work, we apply MD simulations to study the composition-dependent isothermal crystal nucleation in polymer blends, in which the major component is high-density polyethylene (PE). Using simulations, we show that in strongly phase-separated blends of PE and polyethylene oxide (PEO), the crystal nucleation rate of PE at 300K is nearly identical to that in pure samples. In this case, crystal nucleation occurs in the bulk region of the PE domain, away from the impurity phase. This result is consistent with our previous work in which crystalline order nucleated in the PE domain, away from the planar interfaces between phase-separated PE and isotactic polypropylene (iPP), of which the incompatibility was artificially enhanced.[23] When crystallizing from well-mixed blends, the nucleation of crystalline PE is composition-dependent. And the composition dependence is governed by the molecular structures of the impurities. Adding impurities such as isotactic polypropylene, cis-1,4-polybutadiene (cis-PB), and hexyl-branched ethylene-octene copolymer (EOC) slows down PE crystal nucleation. Trans-1,4-polybutadiene (trans-PB), however, imposes negligible effects on PE crystallization.

The impurity polymers hinder crystal nucleation by hampering the formation of nematic precursors. At sufficiently low crystallization temperatures, such as 300K, PE may first form a metastable nematic precursor before crystallization.[24] Crystalline order only nucleates in sufficiently large nematic domains. Thus, adding impurities to polymer blends impedes nematic precursor formation, and in turn, hinder crystal nucleation.

To better understand the role of impurities in PE crystallization, we develop a theoretical model to predict the distributions of impurities and nematic order and the free energy of a critical nematic precursor. We demonstrate that the free energy barrier increases with increasing the volume fraction of impurities with weak nematic interactions, such as iPP. And

the impurity polymers are expelled from PE before the formation of nematic precursors. The predicted composition dependence of the free energy barriers is consistent with the observed composition-dependent nucleation rates in our simulations of PE/iPP and PE/cis-PB blends. When PE is mixed with polymers with sufficiently strong nematic interactions, such as trans-PB, however, the impurities do not impose significant effects on crystal nucleation. Indeed, trans-PB can reduce the free energy barrier for PE to nucleate nematic order. Still, kinetic factors such as polymer relaxation and transport limit the phase transition kinetics even when the free energy barrier is negligible.

Our paper is organized as follows. In the Methods section, we first present the details of simulation setups. We then discuss a theoretical method for obtaining nematic coupling parameters for impurities in PE matrices. In the last part of the Methods section, our theoretical model for predicting the free energy barrier for nucleating nematic order in well-mixed binary blends is discussed. Readers less concerned with the details of our simulations and theoretical model may proceed to the Results and Discussion section, where we compare and discuss our simulations and theoretical predictions.

Methods

Simulation details

In our simulations, we mix high-density polyethylene oligomers (PE) with various thermoplastic oligomers, including isotactic polypropylene (iPP), ethylene-octene copolymer (EOC), trans-1,4- and cis-1,4-polybutadiene (trans- and cis-PB), and polyethylene oxide (PEO), to mimic mechanically recycled PE, in which PE is inevitably contaminated by trace amounts of other plastics. By varying the fractions of octene comonomers, which are evenly distributed along the polymer backbones, two types of EOC are considered, namely EOC-1 (19% octene comonomers) and EOC-2 (34% octene comonomers). Although the other impurities are crystallizable, the hexyl side chains can prevent EOCs from crystallizing.[25] The molecular

details of different polymer samples are summarized in Table 1. To model these blends, we apply the united-atom TraPPE force field,[26,27] which successfully described the condensed phase properties and the crystallization behaviors of n-alkane, alkene, PE and iPP.[24,28–33]

Table 1: Molecular details of different polymer samples. Chain lengths are in degree of polymerization. ϕ is the impurity volume fraction.

Samples	PE length	Impurities length	comonomer fraction	ϕ
PE/iPP	100	100	N/A	0.000-0.205
PE/long iPP	100	200	N/A	0.000-0.205
PE/EOC-1	100	100	0.19	0.000-0.215
PE/EOC-2	100	100	0.34	0.000-0.261
PE/cis-PB	100	50	N/A	0.000-0.231
PE/trans-PB	100	50	N/A	0.000-0.237
PE/PEO	100	66	N/A	0.000-0.210

We prepare the equilibrated melt configurations by NPT simulations at 550K and 1 bar using the GROMACS 2019.2 package.[34] The temperature and pressure couplings are velocity-rescale and Berendsen, respectively. The initial configurations are randomly and loosely packed PE oligomers and minority thermoplastics. Most chains here are of length 200 backbone atoms and the total number of backbone atoms is 40000 for each simulation. We also double the length of iPP oligomers to show that the composition-dependent nucleation in a well-mixed blend relies weakly on impurity molecular weight. After densifying the melt densities under the NPT condition to values of about 0.7 g/cm^3, we equilibrate the polymer blends for 420 ns, much greater than the Rouse relaxation time of the PE oligomers, about 9 ns. Before crystallization, PE and non-polar impurities are randomly mixed. Indeed, high molecular weight PE and iPP can phase separate in experiments. In this work, the relatively short PE and iPP oligomers do not phase separate at 550K due to the rather low Flory-Huggins χ between the two chemically similar species.[35] However, the polar PEO phase separates from PE and forms spherical domains. From each equilibrated trajectory, we extract 15 distinct melt configurations, which are quenched to 300K to trigger isothermal crystal nucleation. To simulate crystal formation, anisotropic Perrinello-Rahman pressure coupling is applied to allow independent fluctuations of simulation boxes in the x, y, and z

directions.

In our simulations, PE can nucleate under quiescent and deep supercooling conditions. To identify the crystalline order during isothermal nucleation, we use a local bond-order parameter $q_6 q_6^*$, which quantifies the correlation among the six-order Steinhardt order parameters of a reference atom and its neighboring atoms within a cut-off distance of 0.54 nm, which corresponds to the location of the first maximum in the pair correlation function of PE atoms.[24,25,36] A local bond order parameter greater than 2.2 can distinguish crystalline atoms of united-atom PE from isotropic ones. The incubation time τ for the critical nuclei to form in pure PE is about 30 ns. The value of τ, however, can increase with increasing the volume fraction of impurity polymers, such as iPP. When the volume fraction of iPP is 0.21, we observe the slowest PE crystal nucleation in our simulations, with an incubation time of about 100 ns. Nevertheless, by performing MD simulations of polymer blends for 200 ns, we can quantify the early-stage nucleation kinetics of PE in the model polymer blends.

In well-mixed polymer blends, impurity polymers can hinder PE crystal nucleation by impeding the formation of metastable nematic precursors. Instead of directly nucleating crystalline order, PE needs to first form sufficiently large nematic precursors, in which crystalline order emerges. To show this, we define the local nematic order of a given atom k:

$$Q_{ij} = \frac{1}{n}\sum_{k=1}^{n}(t_i^k t_j^k - \frac{1}{3}\delta_{ij}) \tag{1}$$

in which n is the total number of atoms within a cut-off distance of 1.08 nm from the reference atom k, t^k is a unit tangent vector across atom k, and indices $i, j = (x, y, z)$. Based on the largest eigenvalue λ of Q, a scalar order parameter $S = 1.5\lambda$ quantifies the local nematic order. We choose the extended cut-off distance of 1.08 nm to include extra neighboring atoms in the calculations and ensure the local nematic order S is close to zero for isotropic atoms. An atom with S greater than 0.39 is considered nematic. By grouping neighboring nematic atoms (within 0.54 nm), we identify nematic nuclei.[24]

The crystalline order of PE indeed prefers to emerge in the center of a large nematic

domain where atoms are highly uniaxially aligned. In Figure 1, we show the growth of the largest nematic nucleus in a pure PE sample at 300K. In small nematic nuclei, S is rather weak and no crystalline order can be observed. As the nematic nucleus grows, its center becomes more uniaxially ordered, and eventually, crystalline order appears in a sufficiently large nematic domain. By hindering the formation of these nematic precursors, impurity polymers such as iPP can impede PE nucleation.

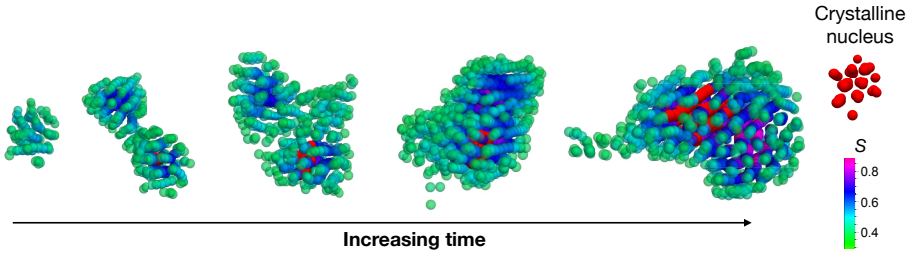

Figure 1: Growth of a nematic nucleus in a pure PE sample. Local order S indicated by color. A crystalline nucleus inside a large nematic domain highlighted in red.

Estimating nematic interactions

The formation of nematic precursors is governed by the nematic coupling interactions between polymer segments. For molten semiflexible chains, the mean-field nematic free energy per monomer is

$$F_{nem} = -\frac{1}{2}\alpha S^2 - T\Delta F_o(S) \tag{2}$$

in which α is the nematic coupling parameter, which quantifies the interaction strength of a monomer segment with the nematic field S. The nematic free energy here can be viewed as the Landau free energy in which α is the expansion coefficient for the quadratic term in nematic order S and the higher order terms are grouped in the orientational entropy loss $\Delta F_o(S)$. The value of $\Delta F_o(S)$ depends on polymer persistence length N_p (in the number of monomer units) and can be obtained using a variational approach.[24] Long semiflexible chains exhibit a first-order isotropic-to-nematic phase transition when $\alpha N_p > 6.67kT$.[24,37,38] For PE, the nematic coupling parameter has an entropic origin – it arises from local molecular

packing and is rather temperature-independent, about 1.7 kT. Above the crystal melting temperature, the persistence length N_p of PE is rather low and thus the polymer chains are isotropic in melts. Because the backbone stiffness N_p increases with decreasing temperature, PE can transition into the meta-stable nematic phase at low crystallization temperatures.

Different molecular structures of the impurity polymers can lead to various nematic interactions. The mismatch in nematic interactions of PE and impurities can impact the free energy barrier for the PE segment to nucleate nematic order in a well-mixed blend. To better understand the role of nematic interactions in PE crystal nucleation, we estimate α for linear impurities that are well-mixed with PE in the melt state using MD simulations and a mean-field theory. Here we do not extract α for EOC chains because the theoretical treatment for branched semiflexible chains is beyond the scope of this manuscript.

To compute α, we first blend small amounts of short impurity chains (molar fraction of 0.05) with PE oligomers in NPT simulations. All the polymer chains have only 40 backbone carbons. The short chain lengths permit the blends to remain well-mixed at temperatures ranging from 550K to 450K. From MD simulations of chains in the isotropic phase, we compute the backbone tangent-tangent correlation functions for the polymer species, from which the temperature-dependent persistence length N_p is obtained: $\langle t_0 \cdot t_i \rangle = \exp(-i/N_p)$, in which t_i is the unit backbone tangent vector across the ith monomer. By measuring the tangent-tangent correlation functions for polymers before crystallization, we also obtain the persistence length for PE, iPP, and cis- and trans-PB at 300K. For PE, iPP, and trans-PB, N_p increases slightly with decreasing temperature (Figure 2). The persistence length of cis-PB is about 1.2 monomers and rather temperature independent, consistent with previous all-atom simulation results.[39] Together with α, N_p governs the nematic interactions of impurity polymers when the sample is quenched to crystallize.

We then apply uniaxial forces f, about 0.19 kT per PE monomer, to stretch the head and end monomers of PE oligomers in opposite directions along the z-axis at various temperatures. The uniaxial tension induced a mean nematic order $S_1 = \langle P_2(t_i \cdot \hat{z}) \rangle$ to PE segments,

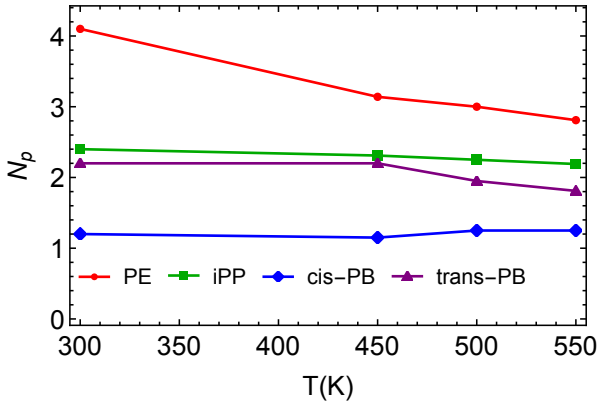

Figure 2: Temperature-dependent persistence length N_p (in number of monomers).

where t_i is the backbone unit vector across monomer i and P_2 is the 2nd-order Legendre Polynomial. By interacting with the uniaxially aligned PE, the impurity chains also exhibit weak nematic order, of which the magnitude is governed by the nematic coupling interactions (Figure 3). The rather weak tension f only leads to mild mismatches in nematic order for PE and impurities, and in turn, avoids the tension-induced phase separation between the stretched and free chains.[40]

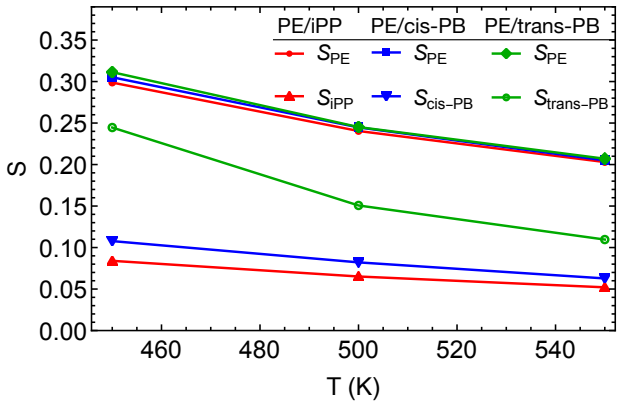

Figure 3: Nematic order S of stretched PE and unstretched impurities at different temperatures.

We can compute the average nematic order for the "probe impurity chains" as a function of their nematic coupling parameter α_2. The single chain Hamiltonian of the semiflexible

impurity polymer of length N in a mean nematic field S is:

$$\frac{H_{impurity}(N)}{kT} = \int_0^N ds \left(\frac{N_p}{2} \left| \frac{dt_s}{ds} \right|^2 - \alpha_2 S P_2(\mu_s) \right) \tag{3}$$

in which k is the Boltzmann constant, T is temperature, t_s is the unit backbone tangent vector across monomer s, $\mu_s = t_s \cdot \hat{z}$, and S is the average nematic order in the system. The value of S depends on the nematic order of PE, S_1, and that of impurities, S_2, as $S = (1-\phi)S_1 + \phi S_2$. At low impurity volume fraction ϕ, mean nematic order in the system arises from the tension-induced ordering of PE and thus we approximate $S \approx S_1$. The stretched PE acts as "nematic solvents" that induce uniaxial ordering to the semiflexible impurities.

Using the single chain Hamiltonian, we write the propagator $z(\mu; N)$ as:

$$z(\mu; N) = \frac{1}{z_0} \int d\mu_1 d\mu_2 ... d\mu_S e^{-H_{impurity}(N)/kT} \delta(\mu_1 - \mu) \tag{4}$$

in which z_0 normalizes the propagator with respect to a free chain. The value of $z(\mu; N)$ states the conditional Boltzmann weight of an impurity chain of length N, starting with backbone tangent orientation μ. The evolution of $z(\mu; s)$ follows a biased diffusion equation:[40–42]

$$\frac{\partial z(\mu; s)}{\partial s} = \left(\frac{1}{2N_p} \nabla_\perp^2 + \beta \alpha_2 S_1 P_2(\mu) \right) z(\mu; s) \tag{5}$$

in which $\nabla_\perp^2$ is the angular Laplacian. The diffusion equation can be solved by expanding $z(\mu; s)$ in the eigenfunctions ψ_i of the right-hand side operator, and then applying the Legendre polynomial expansion to ψ_i.[43]

The orientational distribution of backbone tangent vectors is thus proportional to the product of two propagators, integrated over all the backbone monomers:

$$p(\mu) \propto \int_0^N ds z(\mu; s) z(\mu; N - s) \tag{6}$$

By integrating $P_2(\mu)$ over the distribution $p(\mu)$, we can obtain the nematic order $S_2 = \int d\mu p(\mu) P_2(\mu)$ for the impurity. Using the above equations, we then solve the nematic order S_2 as a function of α_2 for a given background nematic order S_1 (Figure 4a, 4b, and 4c).

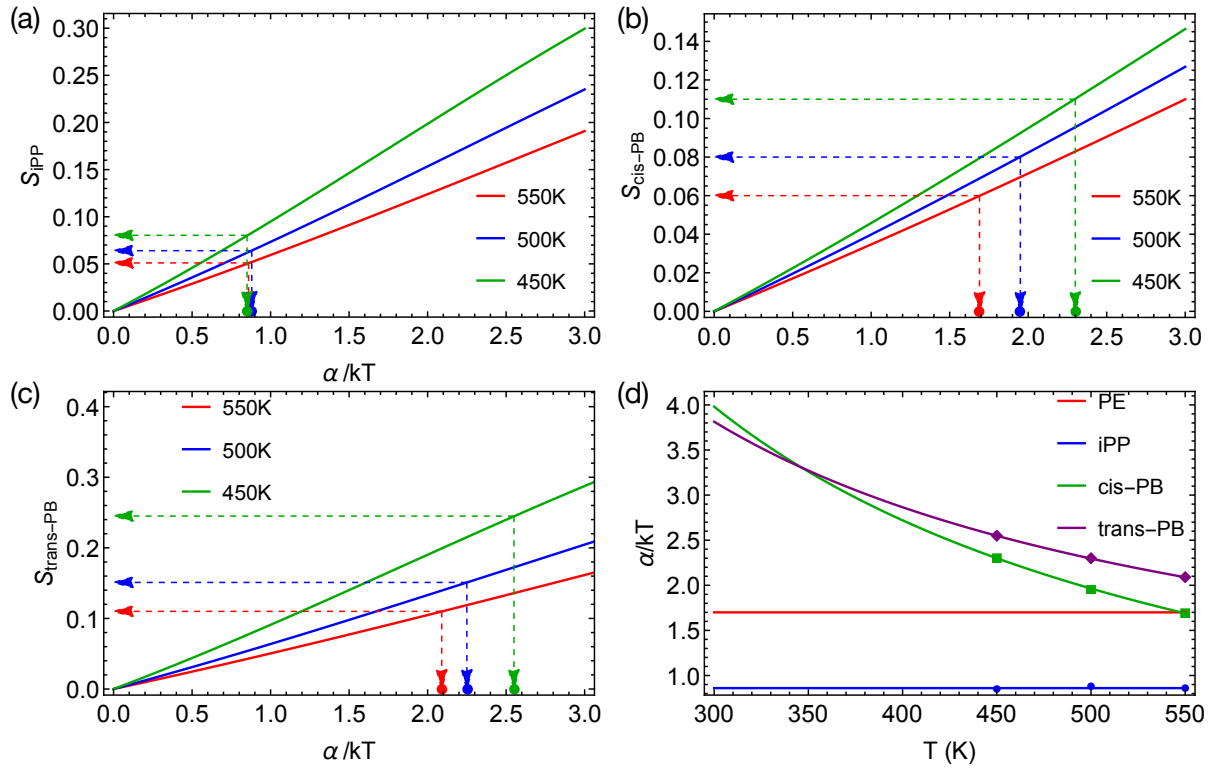

Figure 4: (a) Predicted nematic order S as a function of monomeric nematic coupling parameter α for (a) iPP, (b) cis-PB, and (c) trans-PB in stretched PE matrix. Mean-field prediction (curves). Fitting to MD simulation results (dashed arrows). Disks represent α at different temperatures. (d) Nematic coupling constant α at different temperatures for PE, iPP, cis-PB, and trans-PB. Fits to $\alpha(T) = A + B/T$ (curves). Temperature independent α for PE from Zhang and Larson.[24]

By fitting the calculated nematic order to MD simulation results, we can obtain the nematic coupling parameter for free impurity polymers. Similar to the temperature-independent nematic coupling parameter of PE,[24] α/kT of iPP is also temperature-independent (Figure 4d). However, the nematic coupling parameters of cis-PB and trans-PB increase with increasing temperature. To obtain the nematic coupling constants at 300K, we fit the predicted α of cis-PB and trans-PB to $\alpha = A + B/T$ and perform extrapolations. We later demonstrate that cis-PB exhibits stronger nematic interactions, which in turn, lead to a

weaker hindrance on nematic precursor formation than iPP at 300K.

Free energy barrier for nucleating nematic order in binary blends

The mismatches in the nematic interactions of PE and impurity polymers affect the free energy barriers ΔF_{nem} for nucleating nematic order. To show this, we write the Landau-Ginzburg free energy of a nematic precursor in a binary polymer blend as:

$$\frac{F}{kT} = \int d^3r \left(\frac{\kappa_S}{2} (\nabla S)^2 + \frac{\kappa_\phi}{2} (\nabla \phi_r)^2 + f(\phi_r, S) \right) \tag{7}$$

in which S is the scalar local nematic order, defined using the largest eigenvalue of the nematic order tensor Q (eqn 1) averaged over all the local polymer segments. Together with the local free energy density $f(\phi_r, S)$, the values of κ_S and κ_ϕ govern the sharpness of the orientational and compositional interfaces of the nucleus. In this work, we set $\kappa_S = \kappa_\phi = 1\ nm^{-1}$, which leads to a nematic-isotropic interface with a width of about 1 nm, the same as the persistence length of PE at 300K. We expect the correlation length of the orientational order near the nematic nucleus to be about a persistence length, as predicted by previous theories and simulations.[13,42,44] Because the depletion of impurities occurs in the nematic precursors, we assume κ_{phi} to be the same as κ_s so that the compositional interface is also about 1 nm wide. Quantitatively obtaining κ_S and κ_ϕ requires exhaustive simulations of polymer blends near pre-constructed planar nematic-isotropic interfaces, which are beyond the scope of this paper. Nevertheless, we show later that our theory with the approximated κ_S and κ_ϕ agrees with the MD simulation results.

The local free energy density $f(\phi_r, S)$ is :

$$f(\phi_r, S) = f_{nem}(\phi_r, S) + \frac{(1-\phi_r)\ln(1-\phi_r)}{N_1 \Omega} + \frac{\phi_r \ln \phi_r}{N_2 \Omega} \tag{8}$$

in which f_{nem} is the nematic free energy density for a well-mixed blend, ϕ_r is the local volume fraction of impurities at radial distance r from the center of the nucleus, N_i and Ω are the

chain length and the reference monomer volume, respectively. In this work, we choose Ω as the monomer volume of PE at 300K, of about 0.05 nm^3. The above equation is inspired by the Flory-Huggins theory for polymer blends in which the free energy of mixing is the linear combination of effective repulsion between different species and the translation entropy. Evidently, in eqn 8, we neglect the chemical incompatibility between the two polymers in the melt state. We assume the depletion of impurities from the nematic precursors of PE results is governed by the mismatch in nematic interactions of different polymers. One can easily insert a Flory-Huggins interaction term $\chi\phi_r(1-\phi_r)$ in eqn 8 to include the chemical incompatibility in the free energy functional. Later we demonstrate that χ only impacts the nucleation barrier at high impurity fractions.

To obtain f_{nem} for a well-mixed blend, we first write the nematic free energy for a monomer of polymer i:

$$F^i_{nem}(S_i, S) = -\frac{1}{2}\alpha_i S S_i - T\Delta F^i_o(S_i) \tag{9}$$

where S_i is the nematic order of species i and the local mean nematic field is $S = (1-\eta)S_1 + \eta S_2$, in which η is the molar fraction of the impurity. Assuming the polymers interact separately with the mean nematic field, we approximate the net free energy of the blend as a function of the nematic order of the two polymers using a linear mixing rule:

$$F_{nem}(\eta, S_1, S_2) = (1-\eta)F^1_{nem}(S_1, S) + \eta F^2_{nem}(S_2, S) \tag{10}$$

The free energy of a well-mixed blend represents the saddle path $F^*_{nem}(\eta, S)$ on the free energy surface (Figure 5a). Using the molar volumes Ω_1 and Ω_2 of the two species, we obtain the nematic free energy density of a well-mixed blend:

$$f_{nem}(\phi, S) = \frac{F^*_{nem}(\eta, S)}{(1-\eta)\Omega_1 + \eta\Omega_2} \tag{11}$$

where the volume fraction $\phi = \eta\Omega_2/((1-\eta)\Omega_1 + \eta\Omega_2)$. When PE is mixed with impurity

polymers of weaker nematic interactions, $f_{nem}(\phi_r, S)$ becomes greater with increasing ϕ_r (Figure 5b). A sufficient amount of impurities can even destabilize the metastable nematic phase of PE.

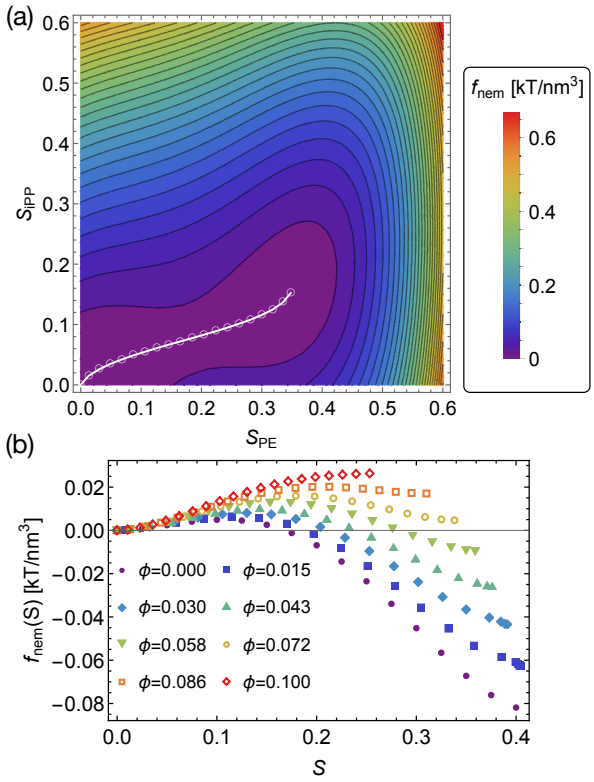

Figure 5: (a) Nematic free energy density f_{nem} for a well-mixed PE/iPP blend with iPP volume fraction $\phi = 0.072$. White symbols and curve represent saddle points and saddle path, respectively. (b) f_{nem} vs. average nematic order S for PE/iPP with various bulk composition ϕ.

Because the critical nucleus represents the maximum free energy along the reaction coordinate, we obtain the nematic order and composition distributions in a critical nematic nucleus by extremizing eqn 7 with respect to the distributions of S and ϕ_r:

$$\begin{aligned} 0 = \frac{\delta F}{\delta S} &= -\kappa_S \nabla^2 S + (1-\phi_r) f_1'(S) + \phi_r f_2'(S) \\ 0 = \frac{\delta F}{\delta \phi_r} + \lambda \frac{\delta}{\delta \phi_r} \int d^3r(\phi_r - \phi) &= -\kappa_\phi \nabla^2 \phi_r - f_1(S) + f_2(S) - \frac{\ln(1-\phi_r)}{N_1 \Omega} + \frac{\ln \phi_r}{N_2 \Omega} + \lambda \end{aligned} \tag{12}$$

in which ϕ is the bulk impurity volume fraction. Here, S is a non-conserved order parameter, and the volume fraction is conserved in the sample. Thus, a Lagrange multiplier λ

is introduced to constrain the overall blend composition. We numerically solve the above differential equations in Mathematica with the boundary conditions: $S'(0) = \phi_r'(0) = 0$, $S(\infty) = 0$, and $\phi_r(\infty) = \phi$. By inserting $S(r)$ and $\phi_r(r)$ into eqn 7, we can compute the free energy of the critical nematic nucleus ΔF_{nem}. Similar approaches have been applied to study the crystal nucleation in metal alloys.[45,46] Using the theoretical model, we will demonstrate later how ΔF_{nem} varies as a function of mismatch in nematic interactions and the bulk impurity fraction ϕ.

Results and discussion

Simulation results

To quantify the nucleation kinetics, we compute the mean-first-passage time (MFPT) for the largest crystalline nucleus of PE to reach size n_{max} carbons by averaging over the different simulation trajectories (Figure 6a). By fitting the classical nucleation theory (CNT)[47] to the MFPT (Figure 6b), we obtain the incubation time τ and the corresponding nucleation rate $I_{cry} = \tau^{-1}V^{-1}$, in which V is the sample volume for well-mixed blends and the PE volume for phase-separated PE/PEO. For PE/PEO blends, I_{cry} is independent of impurity volume fraction ϕ (Figure 6c). In this case, crystal nucleation occurs in the PE domains and thus the nucleation rate is similar to that in pure samples. The result here is consistent with our previous work in which we show crystal nucleation prefers to occur away from the interfaces in phase-separated polymer blends.[23]

In well-mixed polymer blends, I_{cry} decreases with increasing impurity volume fraction (Figure 6c). The composition dependence is governed by the contaminant molecular structures. Among all the polymers studied here, iPP is the most effective in slowing down PE nucleation. Hexyl side groups on EOC, which are incompatible with crystalline PE and prevent EOC from crystallizing,[25] exhibit weaker hindrance on PE nucleation than the crystallizable iPP. The degree of hexyl branches of EOC only imposes a mild effect on PE

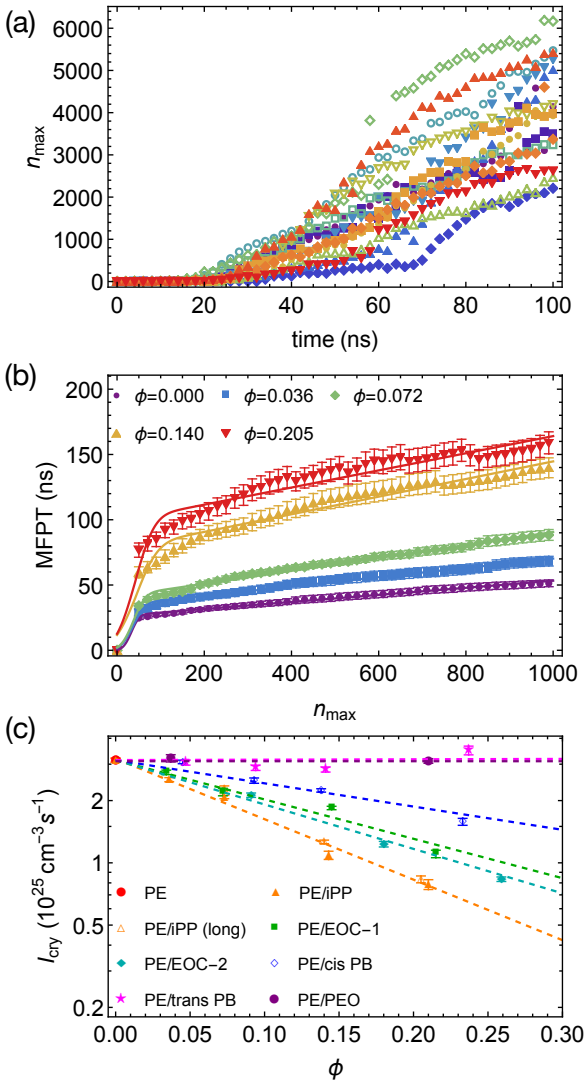

Figure 6: (a) Largest crystal nucleus size n_{max} vs. simulation time t in different pure PE samples. (b) MFPT for the largest crystal nucleus of PE to reach size n_{max} in PE/iPP blends of various iPP volume fraction ϕ. Error bars obtained using bootstrapping. Fits to CNT (curves). (c) Crystal nucleation rate I_{cry} of PE vs. impurity volume fraction ϕ. Exponential fits to guide the eye (dashed lines). Error bars represent the 95% confidence intervals of fitting parameters.

nucleation. Impurities with different geometric isomerism, however, can lead to distinct composition dependence. Although blending PE with cis-PB can hinder PE crystallization, trans-PB imposes negligible effects on PE nucleation. Using iPP with different numbers of backbone carbon atoms (200 and 400), we also demonstrate that the PE nucleation rate only weakly depends on the molecular weight of long impurity chains.

We expect the compositional dependence of the nucleation rate to arise from the mismatch in nematic interactions of different polymers. Using a mean-field theory and MD simulations, we show that different linear polymers in this study exhibit various nematic coupling interactions (Figure 4b). Blending PE with impurities with weaker nematic coupling parameters may reduce the nematic interactions and increase the free energy barrier for nucleating nematic order. At 300K, the crystalline order of PE only nucleates inside sufficiently large nematic precursors. Thus, impurities may impede the overall crystal nucleation by hindering the formation of nematic precursors.

To show impurities can indeed slow down the formation of PE nematic precursors, we perform the MFPT analysis for the formation of the largest nematic nucleus (Figure 7a and 7b) and obtain the nucleation rate I_{nem}, which is greater than the crystal nucleation rate I_{cry}. For blends that contain iPP, cis-PB, and EOC, I_{nem} decreases with increasing impurity volume fraction and the composition-dependence of I_{nem} is similar to that of I_{cry} (Figure 7c). With somewhat stronger nematic interactions, trans-PB imposes negligible effects on nematic precursor formation.

To further demonstrate that the observed composition-dependence of I_{cry} arises from the delayed formation of nematic precursors, we prepare nematic PE/iPP samples in the melt state by uniaxially stretching all the polymer chains along the x-axis ($\hat{x}$). We use forces of 0.25 kT per monomer to stretch the head and tail of each polymer chain in opposite directions along the x-axis ($\hat{x}$). The uniaxial tension induces a mean nematic order $\langle P_2(t \cdot \hat{x})\rangle$ of about 0.38 for PE, where P_2 is the second-order Legendre polynomial, t is a monomer tangent vector, and $\langle\rangle$ denotes averaging over all monomer tangents (Figure 8a). The values of $\langle P_2(t \cdot \hat{x})\rangle$ depend on the strength of the uniaxial tension and the nematic coupling interactions in the melts. iPP indeed reduces the nematic interactions in PE/iPP so that $\langle P_2(t \cdot \hat{x})\rangle$ of PE decreases with increasing ϕ. We then remove the tension forces and let the uniaxially ordered blends crystallize at 300K. In this case, crystalline order directly nucleates inside the bulk nematic samples.

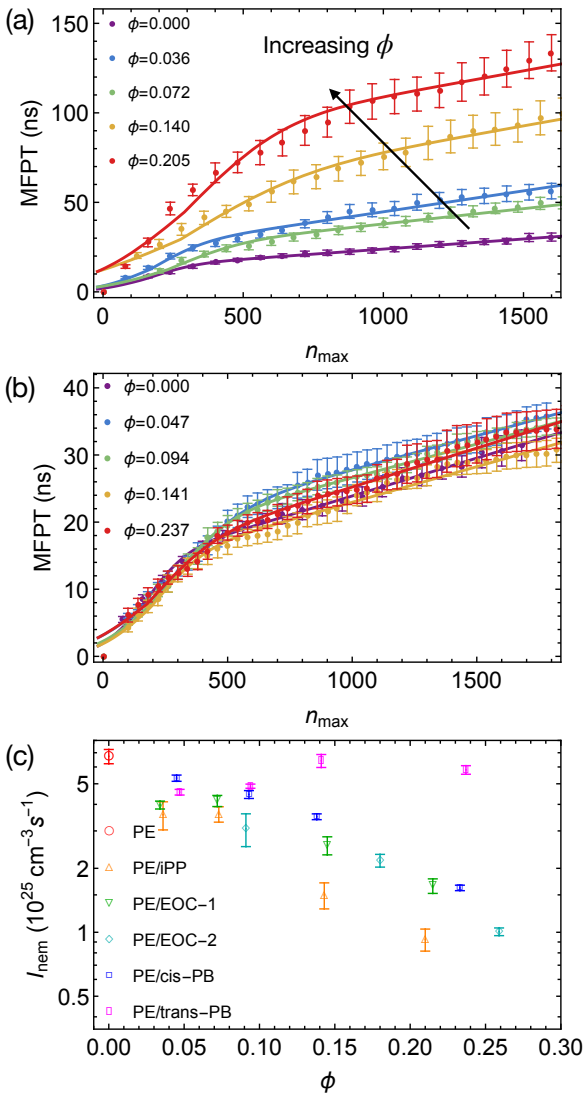

Figure 7: MFPT for the largest nematic nucleus of PE to reach size n_{max} in (a) PE/iPP blends and (b) PE/trans-PB with various impurity volume fractions ϕ. Error bars obtained using bootstrapping. Fits to CNT (curves). (c) Nucleation rate of nematic precursors vs. impurity volume fraction ϕ. Error bars represent the 95% confidence intervals of fitting parameters.

By skipping the induction period for nematic precursors, the formation of a crystalline nucleus is almost instantaneous after the quench, indicating the free energy barrier for nucleating crystalline order is low (Figure 8b). The fast growth of the largest crystalline nucleus cannot be well-described by the classical nucleation theory (CNT). To estimate the short incubation time τ, we fit the growth of the post-critical nucleus to a linear function. By

extrapolating the size of the crystalline nucleus to zero, we estimate τ and the corresponding crystal nucleation rate I_{cry}. When crystallizing from uniaxially ordered blends, I_{cry} of PE exhibits a weaker composition-dependence (Figure 8c). Adding iPP up to a volume fraction of 0.21 leads to a reduction of the PE crystal nucleation rate by a factor of less than two. The different crystal nucleation rates may result from the different initial nematic order of PE in the melt state. Previous work demonstrated that the crystal nucleation rate of PE at 300K increases exponentially with increasing flow-induced nematic order $\langle P_2 \rangle$ before crystallization as $I = I_0 e^{\langle P_2 \rangle / 0.06}$.[10] By removing the subtle effects of tension-induced nematic ordering on crystal nucleation rate, we show that the crystal nucleation of PE in large nematic domains is independent of impurity compositions.

Comparing simulations with theory

In addition to the above simulation evidence, we also use our theoretical model to demonstrate the role of impurities in the formation of nematic precursors. We first consider a symmetric binary polymer blend in which the two polymers are of the same length $N = 100$ and monomer volume $\Omega = 0.05\ nm^{-3}$, which corresponds to the monomer volume of PE at 300K. We set the persistence lengths of the two polymers to be the $N_p = 4.1$, the same as the stiffness of PE at 300K. The nematic coupling parameter for the major component is $\alpha_1 = 1.7\ kT$, also the same as that of PE.[24] At 300K, $\alpha_1 N_p$ is sufficiently large so that the orientational free energy exhibits a global minimum at a finite S, indicating that PE can undergo the first-order isotropic-to-nematic (IN) transition to form a metastable nematic precursor (Figure 5b).

We vary the nematic coupling parameter α_2 of the impurity polymers to show the role of mismatch in nematic interactions in the formation of nematic precursors. When the impurity polymers exhibit a weaker nematic coupling than the main component ($\alpha_2/\alpha_1 < 1$), increasing the volume fraction of impurities leads to greater orientational free energy(Figure 5b). If the nematic coupling interactions of a persistence length segment are sufficiently low

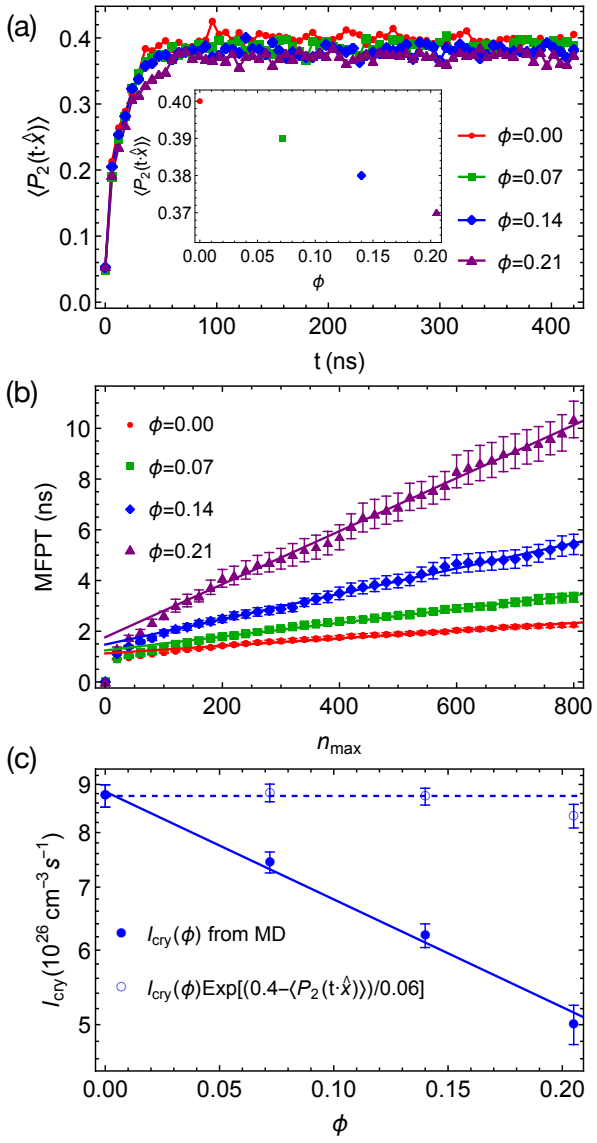

Figure 8: (a) The nematic order of PE in the stretched PE/iPP blends at 550K. Inset: Average nematic order before crystallization vs. iPP fraction ϕ.(b) MFPT for the largest crystal nucleus of PE to reach size n_{max} in uniaxially ordered PE/iPP blends of various iPP volume fraction ϕ. Error bars obtained using bootstrapping. Linear fits (solid lines). (c) Crystal nucleation rates of PE in PE/iPP with stretch-induced nematic order directly from MD simulations (disks) and after correction for different initial nematic order (circles). Solid and dashed lines to guide the eye.

($\alpha_2 N_p < 6.67kT$), the minority polymers cannot undergo the spontaneous IN transition to nucleate the nematic order. Increasing impurity polymers in the blends will eventually destabilize the nematic phase of PE, the major component in the blends. To nucleate nematic order, impurities with weaker nematic interactions are expelled from the critical nematic nu-

cleus. Our theoretical model indeed predicts that ϕ_r in the nematic precursor is lower than the bulk volume fraction ϕ (Figure 9a and 9b). The degree of depletion, however, depends on the mismatch in nematic interactions. Mild mismatch leads to incomplete depletion of the impurities in the critical nematic precursor. With a sufficient mismatch in nematic interactions, the two polymers are not compatible in the nematic phase – the impurities are completely expelled from the nematic precursor. When $\alpha_2/\alpha_1 > 1$, however, the impurities can promote the formation of nematic precursors, and the minority polymers are somewhat enriched in the critical nematic nucleus (Figure 9c).

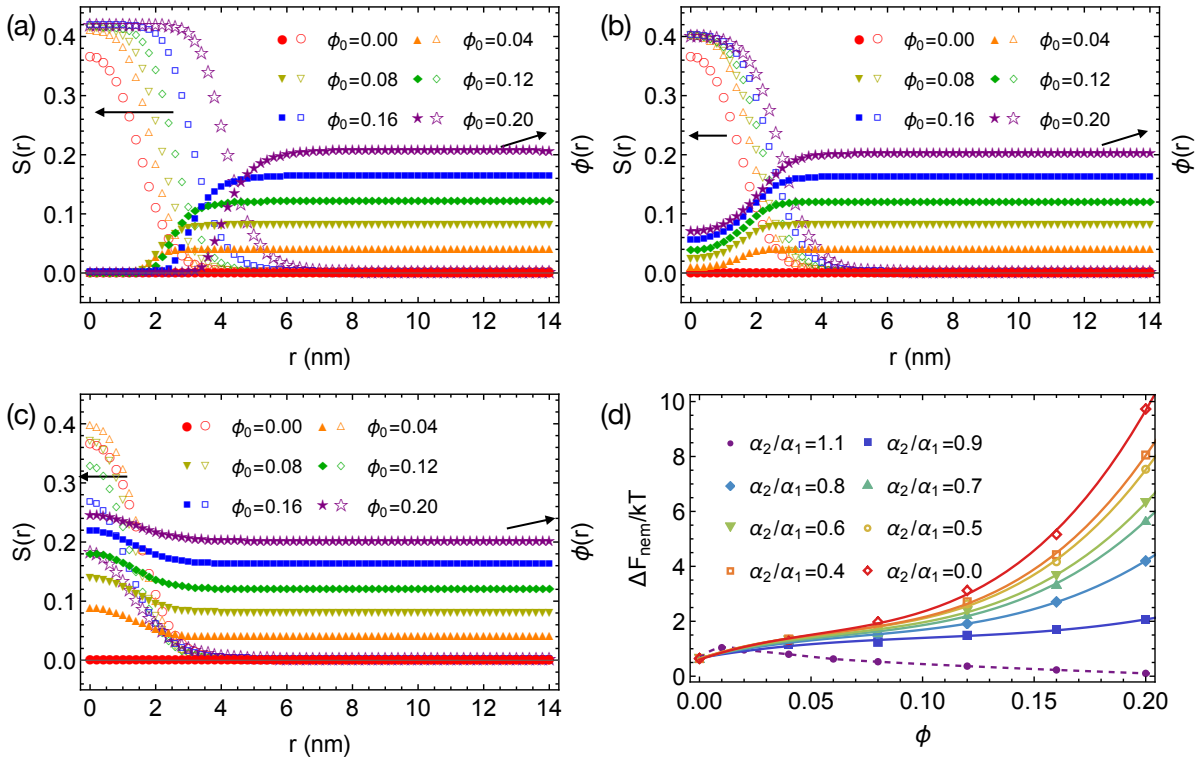

Figure 9: Nematic order (open symbols) and composition profiles (filled symbols) of critical nematic nuclei in symmetric blends with (a) $\alpha_2/\alpha_1 = 0.6$, (b) $\alpha_2/\alpha_1 = 0.9$, (c) $\alpha_2/\alpha_1 = 1.1$, respectively. $r = 0$ represents the center of the nucleus. (d) Free energy barrier for nematic precursor formation ΔF_{nem} vs. impurity volume fraction ϕ. Polynomial fits (solid curves). Interpolation (dashed curve).

By inserting $S(r)$ and $\phi_r(r)$ into eqn 7, we obtain the free energy of the critical nematic nucleus ΔF_{nem}, which increases with ϕ when the impurity polymers weaken the nematic interactions ($\alpha_2/\alpha_1 < 1$) in the blends (Figure 9d). The composition-dependent free energy

barriers can be described using a 3rd-degree polynomial $\Delta F_{nem} \approx \Delta F^0_{nem} + a\phi + b\phi^2 + c\phi^3$, where ΔF^0_{nem} is the free energy barrier for nucleating nematic order in a pure polymer sample. When impurities with stronger nematic interactions ($\alpha_2/\alpha_1 > 1$) are added to the polymer blends, the free energy barrier ΔF_{nem} increases slightly at low ϕ and then decreases with increasing the impurity volume fraction ϕ. Here, adding impurity polymers can promote the formation of nematic precursors. The mild increment of ΔF_{nem} at low ϕ results from the free energy penalty for the compositional gradient at the nematic-melt interface.

We can also use the nematic coupling parameters and persistence lengths measured in MD simulations to compute the free energy barrier for nucleating nematic order in PE/iPP, PE/cis-PB, and PE/trans-PB blends at 300K. Even with zero chemical incompatibility ($\chi = 0$), we predict iPP and cis-PB to be excluded from nematic precursors (Figure 10a and 10b). Blending impurities with weaker nematic interactions can increase the free energy of PE nematic precursors. When the "excess" nematic free energy of mixing in the precursor is sufficiently large to compensate for the reduced translation entropy upon demixing, the impurity polymers are separated from the nematic precursors. With a greater αN_p than that of iPP, a small amount of cis-PB are compatible with nematic PE while iPP is excluded from the nematic precursors. Trans-PB, on the other hand, exhibits stronger nematic coupling interactions than PE. Thus, trans-PB is somewhat enriched in PE nematic precursors. Our theoretical predictions qualitatively agree with MD simulation results. We compute the normalized volume fractions of impurities in nematic precursors with sizes smaller than 1000 carbon atoms in our simulations $\langle\phi_{nem}\rangle/\phi$, where ϕ is the bulk impurity volume fraction (Figure 10d). Indeed, iPP and cis-PB are partially excluded and trans-PB are slightly enriched in nematic domains.

We then compute the free energy barriers for nematic precursor formation ΔF_{nem} as a function of bulk impurity volume fractions ϕ (Figure 11a). The value of ΔF_{nem} increases with increasing ϕ for polymers with nematic interactions weaker than that of PE, such as iPP and cis-PB. With stronger nematic interactions of Kuhn segments, cis-PB chains do not

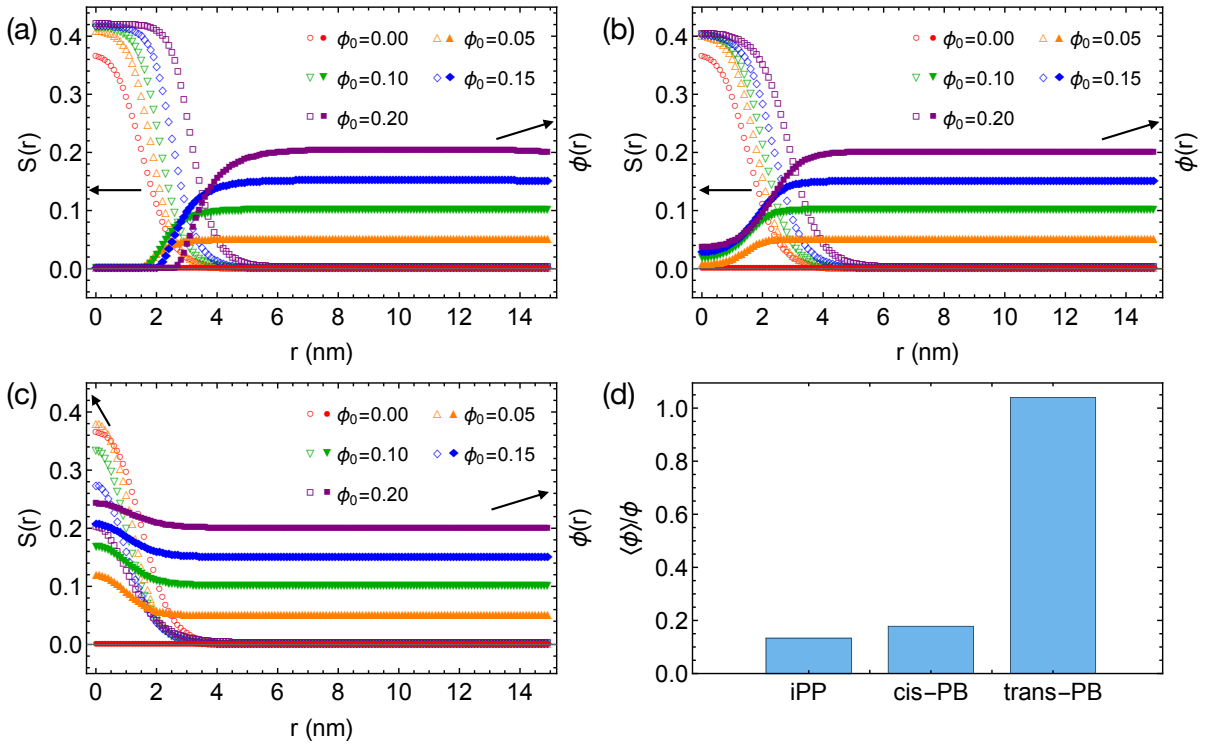

Figure 10: Predicted nematic order (open symbols) and composition profiles (filled symbols) of critical nematic nuclei in (a) PE/iPP, (b) PE/cis-PB, and (c) PE/trans-PB blends. (d) Normalized impurity volume fraction of nematic precursors smaller than 1000 carbon atoms from MD simulations. ϕ denotes bulk volume fraction.

enhance ΔF_{nem} as much as iPP. We expect the nucleation rate of the nematic precursors to decrease exponentially as ΔF_{nem} increases as $I_{nem} = I_0 e^{-\Delta F_{nem}/kT}$, where the pre-exponential factor I_0 depends on the dynamics and transport of polymer segments to the nucleus. Thus, the lower free energy barriers result in a fast and weaker composition-dependent nucleation rate for PE/cis-PB blends, which qualitatively agrees with our MD simulations. Although we predict that adding trans-PB to PE can decrease ΔF_{nem}, the formation rate of nematic precursors in PE/trans-PB remains rather constant as the trans-PB volume fraction increases in the MD simulations. This is because the free energy barrier is already rather low for PE to nucleate the nematic order, of order 1 kT. We expect the formation of nematic precursors in PE/trans-PB is limited by the dynamics and relaxation of polymer chains.

To further validate our theory, we fit the composition-dependent I_{nem} from our simulations for PE/iPP and PE/cis-PB using $I_{nem} = I_0 e^{-\Delta F_{nem}/kT}$, in which ΔF_{nem} is the predicted

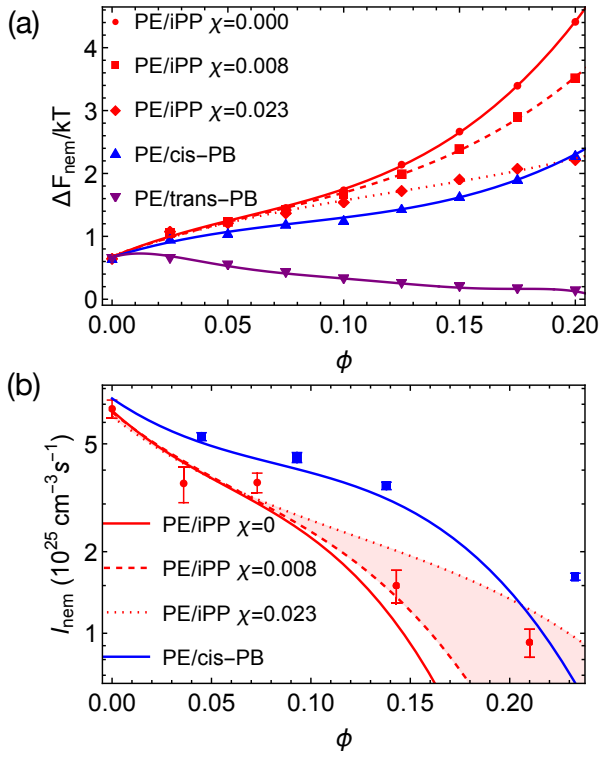

Figure 11: (a) Predicted ΔF_{nem} vs. ϕ for PE/iPP, PE/cis-PB, and PE/trans-PB. χ varies from 0 to 0.023 for PE/iPP and is zero in PE/cis-PB and PE/trans-PB. Polynomial fits (curves). (b) Nucleation rate of nematic precursors I_{nem} vs. ϕ for PE/iPP and PE/cis-PB blends. MD simulations (symbols). Predicted $I_{nem} = I_0 e^{-\Delta F_{nem}/kT}$, where I_0 is the kinetic factor obtained by fitting MD data (curves).

free energy barrier and the kinetic factor I_0 is the only fitting parameter (Figure 11b). Indeed, our theoretically calculated ΔF_{nem} can well describe the composition-dependent I_{nem} at low ϕ. Still, our model overpredicts the free energy barriers at large ϕ for both PE/iPP and PE/cis-PB blends.

The over-prediction arises from the neglected chemical incompatibility between different polymers. In our mean-field model, ΔF_{nem} is essentially the free energy difference between a critical nematic precursor and an isotropic and well-mixed blend, of which the free energy is simply the translation entropy of mixing. In well-mixed polymer blends, the mismatch in molecular structures gives rise to the excess free energy of mixing, often characterized using the Flory-Huggins parameter as $\chi\phi(1-\phi)$. A positive χ penalizes mixing different species and enhances the free energy of a well-mixed blend when the impurity volume fraction ϕ

increases. As a consequence, we expect ΔF_{nem} to be lower at large ϕ when the free energy of the isotropic and well-mixed blend becomes higher due to a positive Flory-Huggins χ.

To demonstrate the effect of χ on ΔF_{nem}, we first estimate χ for PE/iPP blends. Although PE and iPP are common polymers, the experimentally measured χ is not readily available. Nevertheless, we estimate the lower and upper bounds of χ for PE and iPP using the interfacial width between phase-separated PE and iPP, about 3 to 5 nm.[48,49] The Helfand and Tagami theory predicts that the interfacial width for long and incompatible polymer blends as $\xi = 2b/(6\chi)^{1/6}$,[50] where b is the statistical segment length. Using the mean statistical segment length $b = 0.56\ nm$ for PE and iPP,[51] we estimate χ to be in the range of 0.008 to 0.023. We expect the estimated bounds of χ to be reasonable because the Flory-Huggins parameter for PE and head-to-head polypropylene (HHPP) is about 0.009 at 300K,[35] within our predicted range. The upper bound of χ used in this work and the results obtained using inverse gas chromatography are also of the same order of magnitude.[52]

The weak incompatibility between PE and iPP indeed reduces the free energy barrier ΔF_{nem}. By including a positive χ in the free energy functional (eqn 8), we show that ΔF_{nem} decreases with increasing χ. The incompatibility between PE and iPP promotes the depletion of impurities from the nematic precursor. Nevertheless, the effects of χ on ΔF_{nem} are negligible when the impurity volume fraction ϕ is low. Using the lower and upper bounds of ΔF_{nem}, we also obtain the boundaries of the formation rate of nematic precursors in PE/iPP, consistent with our MD simulation results. With correct χ, we expect accurate prediction of the composition-dependent I_{nem} to be feasible for other polymer blends, such as PE/cis-PB.

Finally, we want to point out that the composition-dependent free energy barrier ΔF_{nem} may recall the freezing point depression, a colligative property observed in solutions, for some readers. When the two polymers are incompatible in the nematic phase due to the mismatch in the nematic coupling, the minority polymer must be repelled from the nematic nuclei, which leads to an entropic penalty for demixing. Similar to the effects of solutes on

the freezing points of solvents, the impurities "depress" the isotropic-to-nematic transition temperature and enhance the free energy barrier for nucleating the nematic order. Nevertheless, to quantitatively model the effects of impurity on polymer crystal nucleation, we need the orientational coupling interactions and the incompatibility χ, which are governed by the detailed chemical structures of different components in polymer blends.

Conclusion

In summary, we apply MD simulations to quantify the composition-dependent crystal nucleation of PE in binary blends, which contain small amounts of contaminant polymers. We show that when strong phase separation occurs before crystallization, the crystalline order nucleates in the PE domains, and the nucleation rate I_{cry} is independent of the blend compositions. When PE is mixed with impurity polymers before crystallization, the crystal nucleation rate I_{cry} exhibits a composition dependence. Together with a mean-field model, our simulations demonstrate that impurities with weak nematic coupling, such as iPP, hinder the PE crystal nucleation by increasing the free energy barrier for forming nematic precursors, the prerequisite for PE to nucleate crystalline order at low temperatures. When PE is blended with polymers of strong enough nematic interactions, such as trans-PB, the free energy barrier for nucleation nematic order can be reduced. Kinetic factors, such as transport and conformational relaxation of polymer segments, however, may limit the overall formation rate of the nematic and crystalline nuclei when the free energy barriers are low.

The combination of MD simulations and polymer theories here lays the foundation for predicting the crystal nucleation in polymer blends. The composition-dependent free energy barrier for nucleating the nematic order can be used to approximate the crystal nucleation rate under strong supercooling conditions and permit the prediction of crystallite distributions near the interfaces of weakly phase-separated blends, such as mechanically recycled plastics. We expect our findings to help design better interfacial compatibilizers, such as

multi-block copolymers,[49,53] and optimize the mechanical properties of semicrystalline polymer blends.

Acknowledgement

Support for the NH EPSCoR NH BioMade Project is provided by the National Science Foundation's Research Infrastructure Improvement Award # 1757371. Acknowledgement is also made to the donors of the American Chemical Society Petroleum Research Fund for partial support of this research (# 62491-DNI7).

References

(1) Crist, B.; Fisher, C. J.; Howard, P. R. Mechanical properties of model polyethylenes: tensile elastic modulus and yield stress. *Macromolecules* **1989**, *22*, 1709–1718.

(2) Ward, I. M. Optical and mechanical anisotropy in crystalline polymers. *Proceedings of the Physical Society* **1962**, *80*, 1176.

(3) Gu, K.; Snyder, C. R.; Onorato, J.; Luscombe, C. K.; Bosse, A. W.; Loo, Y.-L. Assessing the Huang–Brown Description of Tie Chains for Charge Transport in Conjugated Polymers. *ACS Macro Letters* **2018**, *7*, 1333–1338.

(4) Lauritzen Jr, J. I.; Hoffman, J. D. Theory of formation of polymer crystals with folded chains in dilute solution. *Journal of research of the National Bureau of Standards. Section A, Physics and chemistry* **1960**, *64*, 73.

(5) Strobl, G. Crystallization and melting of bulk polymers: New observations, conclusions and a thermodynamic scheme. *Progress in polymer science* **2006**, *31*, 398–442.

(6) Erdemir, D.; Lee, A. Y.; Myerson, A. S. Nucleation of crystals from solution: classical and two-step models. *Accounts of chemical research* **2009**, *42*, 621–629.

(7) Sadler, D.; Gilmer, G. A model for chain folding in polymer crystals: rough growth faces are consistent with the observed growth rates. *Polymer* **1984**, *25*, 1446–1452.

(8) Nicholson, D. A.; Rutledge, G. C. An assessment of models for flow-enhanced nucleation in an n-alkane melt by molecular simulation. *Journal of Rheology* **2019**, *63*, 465.

(9) Nicholson, D. A.; Rutledge, G. C. Flow-induced inhomogeneity and enhanced nucleation in a long alkane melt. *Polymer* **2020**, *200*, 122605.

(10) Zhang, W.; Larson, R. G. Effect of Flow-Induced Nematic Order on Polyethylene Crystal Nucleation. *Macromolecules* **2020**, *53*, 7650–7657.

(11) Luo, C.; Sommer, J.-U. Frozen topology: Entanglements control nucleation and crystallization in polymers. *Physical review letters* **2014**, *112*, 195702.

(12) Luo, C.; Sommer, J.-U. Role of thermal history and entanglement related thickness selection in polymer crystallization. *ACS Macro Letters* **2016**, *5*, 30–34.

(13) Hall, K. W.; Percec, S.; Shinoda, W.; Klein, M. L. Property Decoupling across the Embryonic Nucleus–Melt Interface during Polymer Crystal Nucleation. *The Journal of Physical Chemistry B* **2020**, *124*, 4793–4804, DOI: 10.1021/acs.jpcb.0c01972.

(14) Kawak, P.; Banks, D. S.; Tree, D. R. Semiflexible oligomers crystallize via a cooperative phase transition. *The Journal of Chemical Physics* **2021**, *155*, 214902, DOI: 10.1063/5.0067788.

(15) Matsuba, G.; Shimizu, K.; Wang, H.; Wang, Z.; Han, C. C. The effect of phase separation on crystal nucleation density and lamella growth in near-critical polyolefin blends. *Polymer* **2004**, *45*, 5137–5144.

(16) Zhang, X.; Wang, Z.; Muthukumar, M.; Han, C. C. Fluctuation-Assisted Crystallization: In a Simultaneous Phase Separation and Crystallization Polyolefin Blend System. *Macromolecular Rapid Communications* **2005**, *26*, 1285–1288.

(17) Zhang, X.; Wang, Z.; Dong, X.; Wang, D.; Han, C. C. Interplay between two phase transitions: Crystallization and liquid-liquid phase separation in a polyolefin blend. *Journal of Chemical Physics* **2006**, *125*, 024907.

(18) Jin, J.; Du, J.; Chen, H.; Han, C. C. Fluctuation-assisted nucleation in the phase separation/crystallization of iPP/OBC blends. *Polymer* **2011**, *52*, 6161–6172.

(19) Shi, W.; Han, C. C. Dynamic Competition between Crystallization and Phase Separation at the Growth Interface of a PMMA/PEO Blend. *Macromolecules* **2012**, *45*, 336–346.

(20) Arai, F.; Takeshita, H.; Dobashi, M.; Takenaka, K.; Miya, M.; Shiomi, T. Effects of liquid–liquid phase separation on crystallization of poly(ethylene glycol) in blends with isotactic poly(methyl methacrylate). *Polymer* **2012**, *53*, 851–856.

(21) Jin, J.; Chen, H.; Muthukumar, M.; Han, C. C. Kinetics pathway in the phase separation and crystallization of iPP/OBC blends. *Polymer* **2013**, *54*, 4010–4016.

(22) Mitra, M. K.; Muthukumar, M. Theory of spinodal decomposition assisted crystallization in binary mixtures. *Journal of Chemical Physics* **2010**, *132*, 184908.

(23) Zhang, W.; Zou, L. Molecular Dynamics Simulations of Crystal Nucleation near Interfaces in Incompatible Polymer Blends. *Polymers* **2021**, *13*, 347, DOI: 10.3390/polym13030347.

(24) Zhang, W.; Larson, R. G. A metastable nematic precursor accelerates polyethylene oligomer crystallization as determined by atomistic simulations and self-consistent field theory. *Journal of Chemical Physics* **2019**, *150*, 244903.

(25) Zhang, W.; Larson, R. G. Direct All-Atom Molecular Dynamics Simulations of the Effects of Short Chain Branching on Polyethylene Oligomer Crystal Nucleation. *Macromolecules* **2018**, *51*, 4762–4769.

(26) Martin, M. G.; Siepmann, J. I. Transferable Potentials for Phase Equilibria. 1. United-Atom Description of n-Alkanes. *The Journal of Physical Chemistry B* **1998**, *102*, 2569–2577.

(27) Martin, M. G.; Siepmann, J. I. Novel Configurational-Bias Monte Carlo Method for Branched Molecules. Transferable Potentials for Phase Equilibria. 2. United-Atom Description of Branched Alkanes. *The Journal of Physical Chemistry B* **1999**, *103*, 4508–4517.

(28) Wick, C. D.; Martin, M. G.; Siepmann, J. I. Transferable Potentials for Phase Equilibria. 4. United-Atom Description of Linear and Branched Alkenes and Alkylbenzenes. *The Journal of Physical Chemistry B* **2000**, *104*, 8008–8016, DOI: 10.1021/jp001044x.

(29) Karayiannis, N. C.; Mavrantzas, V. G.; Theodorou, D. N. A Novel Monte Carlo Scheme for the Rapid Equilibration of Atomistic Model Polymer Systems of Precisely Defined Molecular Architecture. *Physical Review Letters* **2002**, *88*, 105503.

(30) Foteinopoulou, K.; Karayiannis, N. C.; Laso, M.; Kröger, M. Structure, Dimensions, and Entanglement Statistics of Long Linear Polyethylene Chains. *Journal of Physical Chemistry B* **2009**, *113*, 442–455.

(31) Ramos, J.; Vega, J. F.; Martínez-Salazar, J. Molecular Dynamics Simulations for the Description of Experimental Molecular Conformation, Melt Dynamics, and Phase Transitions in Polyethylene. *Macromolecules* **2015**, *48*, 5016–5027.

(32) Zou, L.; Zhang, W. Molecular Dynamics Simulations of the Effects of Entanglement on Polymer Crystal Nucleation. *Macromolecules* **2022**, *55*, 4899–4906, DOI: 10.1021/acs.macromol.2c00817.

(33) Yamamoto, T. Molecular Dynamics of Crystallization in a Helical Polymer Isotactic Polypropylene from the Oriented Amorphous State. *Macromolecules* **2014**, *47*, 3192–3202.

(34) Hess, B.; Kutzner, C.; van der Spoel, D.; Lindahl, E. GROMACS 4: Algorithms for Highly Efficient, Load-Balanced, and Scalable Molecular Simulation. *Journal of Chemical Theory and Computation* **2008**, *4*, 435–447.

(35) Jeon, H. S.; Lee, J. H.; Balsara, N. P. Predictions of the Thermodynamic Properties of Multicomponent Polyolefin Blends from Measurements on Two-Component Systems. *Macromolecules* **1998-05**, *31*, 3328 – 3339, DOI: 10.1021/ma9709718.

(36) Auer, S.; Frenkel, D. Numerical prediction of absolute crystallization rates in hard-sphere colloids. *The Journal of Chemical Physics* **2004**, *120*, 3015–3029.

(37) Wang, X. J.; Warner, M. Theory of nematic backbone polymer phases and conformations. *Journal of Physics A: Mathematical and General* **1986**, *19*, 2215, DOI: 10.1088/0305-4470/19/11/029.

(38) Ramírez-Hernández, A.; Hur, S.-M.; Armas-Pérez, J.; Cruz, M.; Pablo, J. d. Demixing by a Nematic Mean Field: Coarse-Grained Simulations of Liquid Crystalline Polymers. *Polymers* **2017**, *9*, 88, DOI: 10.3390/polym9030088.

(39) Shetty, S.; Gomez, E. D.; Milner, S. T. Nematic Coupling in Polybutadiene from MD Simulations. *Macromolecules* **2019**, *52*, 528–534, DOI: 10.1021/acs.macromol.8b02209.

(40) Zhang, W.; Larson, R. G. Tension-Induced Nematic Phase Separation in Bidisperse Homopolymer Melts. *ACS Central Science* **2018**, *4*, 1545 – 1550, DOI: 10.1021/acscentsci.8b00651.

(41) Jiang, Y.; Chen, J. Z. Y. Isotropic-Nematic Interface in a Lyotropic System of Wormlike Chains with the Onsager Interaction. *Macromolecules* **2010**, *43*, 10668 – 10678, DOI: 10.1021/ma1022814.

(42) Zhang, W.; Gomez, E. D.; Milner, S. T. Surface-Induced Chain Alignment of Semiflexible Polymers. *Macromolecules* **2016**, *49*, 963–971.

(43) Zhang, W.; Gomez, E. D.; Milner, S. T. Predicting Nematic Phases of Semiflexible Polymers. *Macromolecules* **2015**, *48*, 1454 – 1462, DOI: 10.1021/acs.macromol.5b00013.

(44) Zhang, W.; Gomez, E. D.; Milner, S. T. Using surface-induced ordering to probe the isotropic-to-nematic transition for semiflexible polymers. *Soft Matter* **2016**, *12*, 6141–6147.

(45) Gránásy, L.; Börzsönyi, T.; Pusztai, T. Nucleation and Bulk Crystallization in Binary Phase Field Theory. *Physical Review Letters* **2002**, *88*, 206105, DOI: 10.1103/physrevlett.88.206105.

(46) Gránásy, L.; Tóth, G. I.; Warren, J. A.; Podmaniczky, F.; Tegze, G.; Rátkai, L.; Pusztai, T. Phase-field modeling of crystal nucleation in undercooled liquids – A review. *Progress in Materials Science* **2019**, *106*, 100569, DOI: 10.1016/j.pmatsci.2019.05.002.

(47) Yi, P.; Locker, C. R.; Rutledge, G. C. Molecular Dynamics Simulation of Homogeneous Crystal Nucleation in Polyethylene. *Macromolecules* **2013**, *46*, 4723–4733.

(48) Chaffin, K. A.; Bates, F. S.; Brant, P.; Brown, G. M. Semicrystalline blends of polyethylene and isotactic polypropylene: Improving mechanical performance by enhancing the interfacial structure. *Journal of Polymer Science Part B: Polymer Physics* **2000**, *38*, 108, DOI: 10.1002/(sici)1099-0488(20000101)38:1<108::aid-polb14>3.3.co;2-0.

(49) Xu, J.; Eagan, J. M.; Kim, S.-S.; Pan, S.; Lee, B.; Klimovica, K.; Jin, K.; Lin, T.-W.; Howard, M. J.; Ellison, C. J.; LaPointe, A. M.; Coates, G. W.; Bates, F. S. Compatibilization of Isotactic Polypropylene (iPP) and High-Density Polyethylene (HDPE)

with iPP–PE Multiblock Copolymers. *Macromolecules* **2018**, *51*, 8585–8596, DOI: 10.1021/acs.macromol.8b01907.

(50) Helfand, E.; Tagami, Y. Theory of the Interface between Immiscible Polymers. II. *Journal of Chemical Physics* **1972**, *56*, 3592–3601.

(51) Hiemenz, P. C.; Lodge, T. P. *Polymer Chemistry*; CRC Press: Boca Raton, FL, 2007.

(52) Zhao, L.; Choi, P. Measurement of solvent-independent polymer–polymer Flory–Huggins interaction parameters with the use of non-random partitioning solvents in inverse gas chromatography. *Polymer* **2002**, *43*, 6677–6681, DOI: 10.1016/s0032-3861(02)00673-0.

(53) Eagan, J. M.; Xu, J.; Di Girolamo, R.; Thurber, C. M.; Macosko, C. W.; La-Pointe, A. M.; Bates, F. S.; Coates, G. W. Combining polyethylene and polypropylene: Enhanced performance with PE/iPP multiblock polymers. *Science* **2017**, *355*, 814–816.